# Light-Matter Interactions in Synthetic Magnetic Fields: Landau-Photon Polaritons

Daniele De Bernardis, Ze-Pei Cian, Iacopo Carusotto, Mohammad Hafezi, and Peter Rabl

Phys. Rev. Lett. **126**, 103603 — Published 10 March 2021

DOI: 10.1103/PhysRevLett.126.103603

# Light-matter interactions in synthetic magnetic fields: Landau-photon polaritons


Daniele De Bernardis[1], Ze-Pei Cian[2], Iacopo Carusotto[3], Mohammad Hafezi[2,4], Peter Rabl[1]

[1] *Vienna Center for Quantum Science and Technology, Atominstitut, TU Wien, 1040 Vienna, Austria*

[2] *Joint Quantum Institute, College Park, 20742 MD, USA*

[3] *INO-CNR BEC Center and Dipartimento di Fisica, Università di Trento, I-38123 Povo, Italy and*

[4] *The Institute for Research in Electronics and Applied Physics,*
*University of Maryland, College Park, 20742 MD, USA*



(Dated: December 16, 2020)



We study light-matter interactions in two dimensional photonic systems in the presence of a spatially homogeneous synthetic magnetic field for light. Specifically, we consider one or more two-level emitters located in the bulk region of the lattice, where for increasing magnetic field the photonic modes change from extended plane waves to circulating Landau levels. This change has a drastic effect on the resulting emitter-field dynamics, which becomes intrinsically non-Markovian and chiral, leading to the formation of strongly coupled Landau-photon polaritons. The peculiar dynamical and spectral properties of these quasi-particles can be probed with state-of-the-art photonic lattices in the optical and the microwave domain and may find various applications for the quantum simulation of strongly interacting topological models.


The study of electronic systems in strong magnetic fields has a long tradition in condensed matter physics and led to many important discoveries such as the quantum and the fractional quantum Hall effect or flux quantization in superconducting rings [1, 2]. While for a long time such effects have been restricted to charged particles, over the past years it has been shown that *synthetic* magnetic fields can also be engineered for a variety of neutral systems ranging from atoms in optical lattices [3, 4] to photonic and phononic resonator arrays [5–7]. These systems not only offer the possibility to simulate magnetic fields of unprecedented strength, but also allow us to explore novel phenomena and applications, which are not accessible with electrons. In particular, the ability to interface photons and phonons with atoms or solid-state emitters gives rise to many intriguing questions about the nature of light-matter interactions in magnetic and other topologically non-trivial environments [8–22].

In this Letter we study light-matter interactions in a 2D photonic lattice with an engineered synthetic magnetic field. Several previous works have already addressed the coupling of two-level systems to the chiral edge modes [8, 15–17, 19], which can be used to transport classical or quantum information in a robust and unidirectional way [15, 17, 19, 23, 24]. Here we are interested in emitters coupled to the *bulk* region of the photonic lattice, where the presence of magnetic fields has dramatic consequences on the dynamics of the light emission process. Intuitively, this can be understood from the fact that an emitted photon cannot propagate away, but it is constrained to orbit around the emitter due to the effective Lorentz force [25, 26]. More formally, the formation of photonic Landau levels results in a highly spiked density of states, such that even in an infinite and broad-band lattice, emitter-field interactions become intrinsically non-Markovian at *all* frequencies and coupling strengths. We show that such peculiar conditions lead to a novel kind of excitations that we name Landau-photon polaritons (LPPs). By being composed of circulating [27] and dispersionless, but still spatially extended photons, the spectral and dynamical features of these quasi-particles can be continuously tuned from a single-mode, cavity QED type behavior to that of a many-body system of strongly interacting particles in the presence of a magnetic field. For intermediate parameter settings the hybridization of chiral photons and highly non-linear emitters results in a whole zoo of interacting magnetic lattice models, which are unprecedented in other light-matter or condensed-matter systems. This makes such systems particularly interesting for quantum simulation applications.

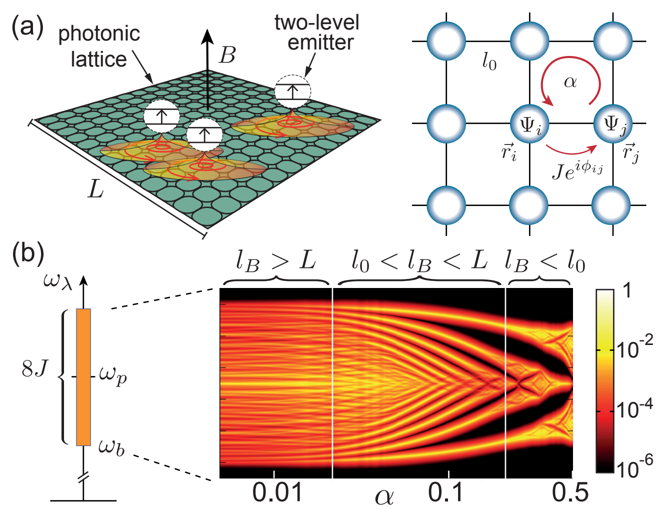


FIG. 1. (a) Sketch of a system of two-level emitters coupled to a photonic lattice with a synthetic magnetic field $B$. The magnetic field is implemented by adjusting the hopping phases $\phi_{ij}$ between neighbouring lattice sites such that around each plaquette $\sum_\square \phi_{ij} = 2\pi\alpha$. (b) The projected density of states, $\rho(\vec{r}_e, \omega)$, is plotted on a logarithmic scale (arbitrary units) as a function of $\alpha$ and for a lattice of $M = 20 \times 20$ sites. For this plot, $\vec{r}_e/l_0 = (10, 10)$ and each resonance is represented by a broadened $\delta$-function with a finite width of $\gamma/J \approx 10^{-3}$.

*Model.*—We consider a setup as shown in Fig. 1(a), where $N$ (artificial) two-level emitters with frequency $\omega_e$ are coupled to a 2D photonic resonator array of length $L$, lattice positions $\vec{r}_i = (x_i, y_i)$ and spacing $l_0$. Each lattice site is represented by a localized photonic mode with frequency $\omega_p$ and annihilation operator $\Psi_i \equiv \Psi(\vec{r}_i)$. Neighboring lattice sites are coupled via the complex tunneling amplitudes $J_{ij} = Je^{i\phi_{ij}}$. The photonic lattice is modelled by the tight-binding Hamiltonian ($\hbar = 1$)

$$H_{\rm ph} = \omega_p \sum_{i=1}^{M} \Psi_i^\dagger \Psi_i - J \sum_{\langle i,j\rangle} \left( e^{i\phi_{ij}} \Psi_i^\dagger \Psi_j + \text{H.c.} \right), \quad (1)$$

where $M = (L/l_0)^2$ is the total number of lattice sites. The Hamiltonian for the combined system is

$$H = H_{\rm ph} + \sum_{n=1}^{N} \frac{\omega_e}{2} \sigma_z^n + g \left[ \Psi(\vec{r}_e^{\,n}) \sigma_+^n + \Psi^\dagger(\vec{r}_e^{\,n}) \sigma_-^n \right], \quad (2)$$

where the $\sigma_k^n$ are the Pauli operators for an emitter at site $\vec{r}_e^{\,n}$ and $g$ is the emitter-field coupling strength.

*A magnetic photonic lattice.*—We are interested in the regime $N \ll M$, where a few emitters are coupled to the bulk region of a much larger photonic lattice. In a standard lattice, where $\phi_{ij} = 0$, $H_{\rm ph}$ can be diagonalised by introducing the annihilation operators $\Psi_\lambda = \sum_i f_\lambda^*(i) \Psi_i$, where the mode functions $f_\lambda(i) \sim e^{i\vec{k}_\lambda \cdot \vec{r}_i}$ are plane waves and the corresponding mode frequencies $\omega_\lambda$ form a continuous band of width $8J$ centred around $\omega_p$ [see Fig. 1(b)]. For $\omega_e$ within this band and $g \ll J$, an excited emitter coupled to this continuum of modes simply undergoes an exponential decay.

Here we consider a lattice where $\phi_{ij} = \frac{e}{\hbar} \int_{\vec{r}_j}^{\vec{r}_i} \vec{A}(\vec{r}) \cdot d\vec{r}$, with $\vec{A}(\vec{r}) = B(-y/2, x/2, 0)$. This arrangement of phases mimics the lattice Hamiltonian for particles with charge $e$ in a homogeneous magnetic field $B$ and thus represents an equivalent synthetic magnetic field for the photons. Such a scenario can be realized, for example, by imposing the tunneling phases through external driving fields [7, 28, 29], by engineering multi-mode lattices with effective spin-orbit interactions [10, 24, 30, 31] or by weakly hybridizing photons with magnetic materials [11, 32] to break time-reversal symmetry. See Ref. [5] for a more detailed discussion of those experimental techniques.

In Fig. 1(b) we plot the projected density of states, $\rho(\vec{r}_e, \omega) = \sum_\lambda |f_\lambda(\vec{r}_e)|^2 \delta(\omega - \omega_\lambda)$, as a function of $\alpha = e\Phi/(2\pi\hbar)$, where $\Phi = Bl_0^2$ is the flux enclosed in a single plaquette. This quantity captures the relevant photonic modes to which an emitter located at $\vec{r}_e$ is coupled to. We identify three different regimes. For very small $\alpha$ the magnetic length $l_B \simeq l_0/(\sqrt{2\pi\alpha})$ exceeds the size of the lattice, $L$. Magnetic effects are not yet important and $\rho(\vec{r}_e, \omega)$ recovers the relatively flat shape of a trivial lattice. In the opposite strong-field regime, $l_B \lesssim l_0$, the magnetic length is comparable to the lattice spacing and $\rho(\vec{r}_e, \omega)$ reproduces the fractal structure of the Hofstadter butterfly [33].

Most relevant for the current discussion is the intermediate regime, where $l_0 < l_B < L$. In this parameter range the discreteness of the lattice is not important and we can use an effective continuum theory, where the eigenmodes $f_\lambda(i) \equiv \Phi_{\ell k}(\vec{r}_i)$ are the usual Landau orbitals [25, 34],

$$\Phi_{\ell k}(\vec{r}_i) \simeq \frac{l_0}{\sqrt{2\pi} l_B} \sqrt{\frac{\ell!}{k!}} \xi_i^{k-\ell} e^{-\frac{|\xi_i|^2}{2}} L_\ell^{k-\ell}\left(|\xi_i|^2\right) \quad (3)$$

with $\xi_i = (x_i + iy_i)/\sqrt{2l_B^2}$ and $L_\ell^{k-\ell}(x)$ are generalized Laguerre polynomials. The index $\ell = 0, 1, 2, \ldots$ labels the discrete Landau levels with frequencies $\omega_\ell \approx \omega_b + \omega_c(\ell + 1/2)$ [34], where $\omega_b = \omega_p - 4J$ is the frequency of the lower band edge and $\omega_c = 4\pi\alpha J$ is the cyclotron frequency. The second index $k = 0, 1, 2 \ldots$ labels the $\sim \alpha M$ degenerate modes within each band. Clearly, both the transformation from a continuous to a discrete spectrum and the localization of the photonic eigenmodes will strongly affect the physics of light-matter interactions in such a synthetic magnetic environment.

*Single-emitter dynamics.*—We first consider the case of a single emitter located at position $\vec{r}_e$ in the bulk of the lattice. The emitter is initially prepared in its excited state and the system's wavefunction can be written as $|\psi\rangle(t) = e^{-i\omega_e t}[c_e(t)\sigma_+ + \sum_i \varphi(\vec{r}_i, t)\Psi^\dagger(\vec{r}_i)]|g\rangle|\text{vac}\rangle$, where $c_e(t)$ is the emitter amplitude and $\varphi(\vec{r}_i, t)$ the photon wavefunction. From this ansatz we obtain

$$\dot{c}_e(t) = -g^2 \int_0^t ds\, G(t - s, \vec{r}_e, \vec{r}_e) c_e(s) e^{i\omega_e(t-s)}, \quad (4)$$

where $G(\tau, \vec{r}_i, \vec{r}_j) = \langle \text{vac}|\Psi(\vec{r}_i, \tau)\Psi^\dagger(\vec{r}_j, 0)|\text{vac}\rangle = \sum_\lambda f_\lambda(\vec{r}_i) f_\lambda^*(\vec{r}_j) e^{-i\omega_\lambda \tau}$ is the photonic Green's function.

In Fig. 2(a) we show the evolution of the excited-state population, $p_e(t) = |c_e(t)|^2$, for different $\alpha$ and different detunings from the band edge, $\delta_e = \omega_e - \omega_b$. For $\alpha = 0$ and $M \to \infty$ the Green's function $G(\tau, \vec{r}_e, \vec{r}_e)$ is represented by a mode continuum and decays on a short time scale, $J^{-1}$. It is then valid to make a Markov approximation and, consistent with a numerical simulation of the full wavefunction $|\psi\rangle(t)$, we obtain an exponential decay of $p_e(t)$ with a rate $\Gamma \simeq 2\pi g^2 \rho(\vec{r}_e, \omega_e) \approx g^2/(2J)$ [34]. For $\alpha \neq 0$ the situation is very different and depending on $\omega_e$ we observe either no decay at all or coherent oscillations. This behaviour can be understood from the exact spectrum of $H_{\rm ph}$ plotted in Fig. 2(b). It exhibits discrete plateaus at frequencies $\omega_\ell$ connected by a sparse set of intermediate modes representing the edge states. Since an emitter in the bulk does not see the edges, whenever $|\omega_e - \omega_\ell| \gtrsim g$ there are no available modes to couple to and the emitter remains frozen in the excited state.

The situation is very different when $\omega_e \simeq \omega_\ell$, in which case the emitter couples to a flat band without dispersion. We can then project the Green's function on the resonant Landau level and obtain $G(\tau, \vec{r}_i, \vec{r}_j) \simeq G_\ell(\vec{r}_i, \vec{r}_j) e^{-i\omega_\ell \tau}$, where

$$G_\ell(\vec{r}_i, \vec{r}_j) \simeq \sqrt{\alpha} e^{i\theta_{ij}} \Phi_{\ell\ell}(\vec{r}_i - \vec{r}_j) \quad (5)$$

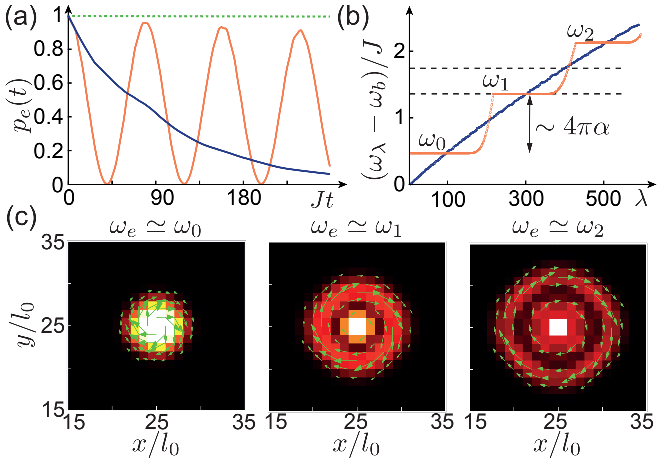


FIG. 2. (a) Evolution of the excited-state population, $p_e(t)$, of an emitter located at $\vec{r}_e/l_0 = (25, 25)$ in a lattice of $50 \times 50$ sites. The parameters are $\alpha = 0$ and $\delta_e/J = 1.35$ (blue line), $\alpha = 0.08$ and $\delta_e/J = 1.35$ (orange line), and $\alpha = 0.08$ and $\delta_e/J = 1.76$ (green dashed line). (b) Plot of the lowest eigenfrequencies $\omega_\lambda$ of the two photonic lattices as used for the simulation shown in blue and orange in (a). The dashed black lines indicate the corresponding emitter's frequencies. (c) Photon density, $|\varphi(\vec{r}_i, t_\pi)|^2$, combined with the profile of the photon current, $\langle \vec{j}_p \rangle(\vec{r}_i, t_\pi)$, at time $t_\pi = \pi/(2\Omega)$, for $\alpha = 0.08$ and $\omega_e = \omega_{\ell=0,1,2}$. For all plots $g/J = 0.14$ and for each lattice site in the bulk (on the edge) a photon decay rate of $\gamma_p/J = 4 \times 10^{-4}$ ($\gamma_{\rm edge}/J \sim 10^{-1}$) has been introduced [34].

and $\theta_{ij} = -(x_i y_j - x_j y_i)/(2l_B^2)$ [34]. Under this approximation, Eq. (4) can be converted into a second-order differential equation, $\ddot{c}_e = -\Omega^2 c_e$. Here

$$\Omega = \sqrt{\alpha} g \tag{6}$$

is the vacuum Rabi frequency, which has the same value for all Landau levels. The predicted Rabi oscillations, $p_e(t) = \cos^2(\Omega t)$, are exactly reproduced by the full numerical simulation, keeping in mind that in Fig. 2(a) we have included a finite loss rate $\gamma_p$ for all photons to describe a realistic scenario. For the photon wavefunction we obtain

$$\varphi(\vec{r}_i, t) = -i \frac{\sin(\Omega t)}{\sqrt{\alpha}} G_\ell(\vec{r}_i, \vec{r}_e), \tag{7}$$

i.e., at time $t_\pi = \pi/(2\Omega)$ the excitation is fully converted into a circulating photon in the Landau orbital $\sim \Phi_{\ell\ell}(\vec{r}_i - \vec{r}_e)$, centered around the emitter. This is shown in Fig. 2(c) in terms of the density, $|\varphi(\vec{r}_i, t_\pi)|^2$, and the photon-current profile, $\langle \vec{j}_p \rangle(\vec{r}_i, t_\pi)$ [34]. Note that all these results are independent of the gauge for $\vec{A}$ and the chosen Landau basis in Eq. (3), which depends explicitly on the origin of the coordinate system. However, $G_\ell(\vec{r}_i, \vec{r}_j)$ still includes a gauge-dependent phase factor, $\theta_{ij}$, which will become important in the following.

*Landau-photon polaritons.*—Let us now extend these results to multiple emitters, still focusing on the regime $\omega_c \gg g$, where the emitters couple dominantly to a single Landau level. In this case each emitter only interacts with photons in the orbital centered around its location, $\Phi_{\ell\ell}(\vec{r}_i - \vec{r}_e^{\,n})$. The photons themselves do not evolve, because there is no dispersion. These special conditions allow us to restrict the dynamics of the whole lattice to a reduced set of modes with bosonic operators

$$B_{\ell n} = \sum_{m=1}^{N} (K^{-1})_{nm} \sum_i G_\ell(\vec{r}_e^{\,m}, \vec{r}_i) \Psi(\vec{r}_i). \tag{8}$$

Here, the $N \times N$ matrix $K$ satisfies $(KK^\dagger)_{nm} = G_\ell(\vec{r}_e^{\,n}, \vec{r}_e^{\,m})$ [34], which ensures that the $B_{\ell n}$ form an orthogonal set of modes with $[B_{\ell n}, B_{\ell m}^\dagger] = \delta_{nm}$. Projected onto these modified Landau orbitals, we obtain the effective Hamiltonian

$$\begin{aligned} H_{\rm LPP}^{(\ell)} =& \omega_\ell \sum_{n=1}^{N} B_{\ell n}^\dagger B_{\ell n} + \frac{\omega_e}{2} \sum_{n=1}^{N} \sigma_z^n \\ &+ g \sum_{n,m=1}^{N} \left( \sigma_+^n K_{nm} B_{\ell m} + B_{\ell m}^\dagger K_{nm}^* \sigma_-^n \right). \end{aligned} \tag{9}$$

It describes the full nonlinear dynamics of LPPs, which are the quasi-particles formed by the coupling of two-level emitters to photons in a single Landau level. This model generalizes the dressed emitter-emitter interactions introduced in [44] and holds even in the presence of a finite bandwidth $J_\ell$ or local frequency disorder $\Delta\omega_p$ [45], as long as $\omega_c \gg g \gg J_\ell, \Delta\omega_p$ [34]. Importantly, $H_{\rm LPP}^{(\ell)}$ only involves $N$ independent photonic modes, i.e., considerably fewer than the number of lattice sites. This makes few-excitation physics numerically tractable, which usually is not possible in 2D waveguide QED systems. In Fig. 3(a) we show the single- and two-excitation spectrum of $H_{\rm LPP}^{(\ell=1)}$ for $N = 3$ equally spaced emitters with $|\vec{r}_e^{\,n} - \vec{r}_e^{\,m}| = d$ and assuming resonance conditions, $\omega_e = \omega_{\ell=1}$.

For a single excitation we obtain an upper and a lower polariton branch, which split into subbands of frequencies

$$\omega_{\ell,\nu}^{\pm} = \omega_e \pm \Omega \sqrt{1 + e^{-\frac{d^2}{4l_B^2}} L_\ell^0\left(\frac{d^2}{2l_B^2}\right) \lambda_\nu}, \tag{10}$$

where $\lambda_{\nu=1,2,3} = 2\cos[(\theta_\triangle + 2\pi\nu)/3]$ and $\theta_\triangle = \theta_{12} + \theta_{23} + \theta_{31} = eBA_\triangle/\hbar$ is the normalized flux through the area $A_\triangle$ enclosed by the three emitters. For widely separated emitters, each emitter supports an independent pair of upper/lower polariton states with the same Rabi splitting $2\Omega$. When the spacing $d$ between emitters is reduced, the photonic wavefunctions start to overlap and each polariton manifold splits into three branches, similar to the formation of binding and anti-binding orbitals in molecules. The dependence on both the enclosed flux as well as on the shape of the Laguerre polynomials quantifying the wavefunction overlap make the spectra of LPPs rather complex. The $\lambda_\nu$ reflect the characteristic eigenvalue structure of a three-site lattice in a magnetic field

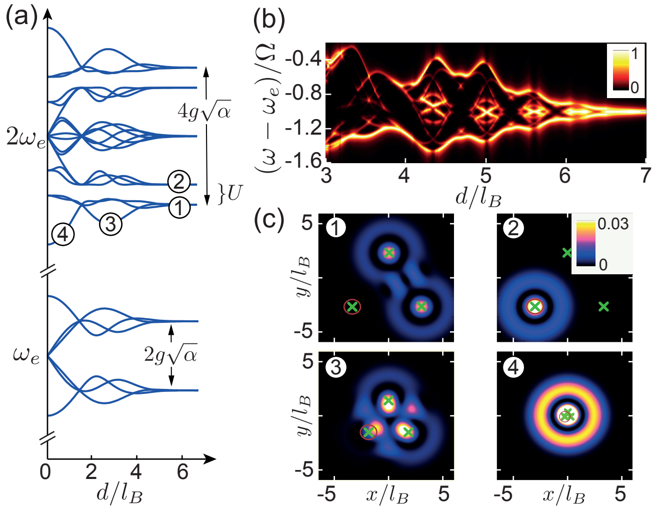


FIG. 3. (a) The spectrum of $H^{(\ell)}_{\rm LPP}$ in the single- and two-excitation sector for $N=3$ equidistant emitters with varying spacing $d$ and for $\ell=1$ and $\omega_e=\omega_1$. (b) Zoom of the lower polaritonic band of the emitter's excitation spectrum, $\mathcal{S}^n_e(\omega)$, for a $N=4\times4$ square lattice of emitters with open boundaries, where $\vec{r}^{\,n}_e$ is the location one of the four inner emitters (the full spectrum is reflection symmetric around $\omega_e$). For this plot, $\alpha=0.08$, $\gamma_e/\Omega=0.02$ and $\ell=3$. The color scale is normalised to the maximum value. (c) Plot of the two-photon correlation function $C(\vec{r}_i,\vec{r}^{\,1}_e)$ for the different two-photon eigenstates indicated in (a). The green crosses represent the emitters position, and the red circle marks the reference emitter's position $\vec{r}^{\,1}_e$ .

and the symmetry between the upper and lower polaritons is a consequence of the resonant coupling of the emitters to a single and degenerate Landau level. For any $\theta_\triangle\neq n\pi$, the left- and right-circulating polariton modes are no longer degenerate, which indicates chirality of LPP propagation [32].

The physics is even richer in large lattices, as exemplified in Fig. 3(b) for a square lattice of $N=4\times4$ emitters. This plot shows the lower part of the emitter's excitation spectrum,

$$\mathcal{S}^n_e(\omega)=\left|\langle G|\sigma^n_-\frac{1}{H-\omega-i\frac{\gamma_e}{2}\sum_m\sigma^m_+\sigma^m_-}\sigma^n_+|G\rangle\right|^2, \quad (11)$$

where $|G\rangle$ is the ground state and $\gamma_e$ is the bare decay rate of the emitters. The repetitive features in this spectrum can be understood in terms of a Harper-Hofstadter model with a flux $\sim d^2/l_B^2$ per plaquette. This spectrum can be directly obtained by detecting the light scattered from one weakly driven emitter.

Let us move to the multiple excitation case. It is well-known that in a single-mode system, the Jaynes-Cummings interaction gives rise to an effective repulsion, $U=\Omega(2-\sqrt{2})$, between two polaritons. This interaction can also be clearly identified in Fig. 3(a), where at large distance $d$ the lowest three eigenstates in the two-excitation sector are separated by $U$ from the next three levels. The difference between these two sets of polaritonic states can be visualized in terms of the two-photon correlation function, $C(\vec{r}_i,\vec{r}_j)=\langle\Psi^\dagger(\vec{r}_j)\Psi^\dagger(\vec{r}_i)\Psi(\vec{r}_i)\Psi(\vec{r}_j)\rangle/\langle\Psi^\dagger(\vec{r}_j)\Psi(\vec{r}_j)\rangle$, plotted in Fig. 3(c). For $d\gg l_B$, the energetically lowest states exhibit strong anti-bunching, $C(\vec{r}_i,\vec{r}_j)\simeq0$ for $|\vec{r}_i-\vec{r}_j|\lesssim l_B$, reminiscent of a Laughlin wavefunction, where particles avoid each other. For the interacting states we obtain $C(\vec{r}^{\,n}_e,\vec{r}^{\,m}_e)\simeq0$ for $n\neq m$, meaning that both photons occupy the same orbital. At smaller distances, the kinetic energy, i.e., the overlap between orbital states becomes more relevant and anti-bunching gradually disappears with details depending on the enclosed magnetic flux, $\theta_\triangle$. For $d\leq l_B$, the emitters couple identically to the field, such that the interactions become fully collective and the spectrum converges to that of a single-mode Tavis-Cummings model [46].

*Chiral dipole-dipole interactions and effective flat-band models.*—The situation is most transparent and intriguing when the emitters are sufficiently detuned from the nearest Landau level, $|\omega_e-\omega_\ell|\gg g$. In this case they are only weakly dressed by the photons, which gives rise to effective dipole-dipole interactions of the form $H_{\rm eff}=\sum_{n,m}\left(\tilde{J}_{nm}\sigma^n_+\sigma^m_-+{\rm H.c.}\right)$. Here

$$\tilde{J}_{nm}\simeq\frac{g^2}{\omega_e-\omega_\ell}|G_\ell(\vec{r}^{\,n}_e,\vec{r}^{\,m}_e)|e^{i\theta_{nm}}, \quad (12)$$

are complex hopping amplitudes, which inherit the magnetic features from the photons. Therefore, also in this almost decoupled limit, dipole-dipole interactions between $N\geq3$ emitters depend sensitively on the magnetic flux, which can lead to a fully chiral transport of excitations. As illustrated in Fig. 4(a), a single excitation flows in the clockwise direction, while two excitations lead to an anti-clockwise dynamics for their relative hole [29].

More generally, the effective Hamiltonian $H_{\rm eff}$ can be viewed as a magnetic lattice model for hard-core bosons, with various additional interesting features. Analogously to Fig. 3, the magnetic flux associated with the phases $\theta_{ij}$ depends on the emitter's arrangement and can be considerably enhanced, i.e., $\alpha_{\rm eff}=\alpha(d/l_0)^2$ for a square lattice. Further, tunneling is no longer constrained to nearest neighbors and depending on the spacing, the lattice geometry and the Landau-level index $\ell$, a whole zoo of magnetic models with different band-structures and field strengths can be realized. For example, in Fig. 4(b) we show the single-excitation spectrum of $H_{\rm eff}$ for a square lattice of emitters for two different spacings, but equivalent effective field strengths. In the first case, only nearest-neighbor couplings are relevant and we recover the regular Hofstadter butterfly with $\alpha_{\rm eff}\approx2.32$ (which is equivalent to $\alpha_{\rm eff}\approx0.32$). In the second example, long-range hoppings are important and the spectrum of the bulk modes becomes essentially flat. This situation is reminiscent of the spectrum of the Kapit-Muller Hamiltonian [47], a prototype toy model for strongly interacting magnetic systems. Interestingly, such abstract models

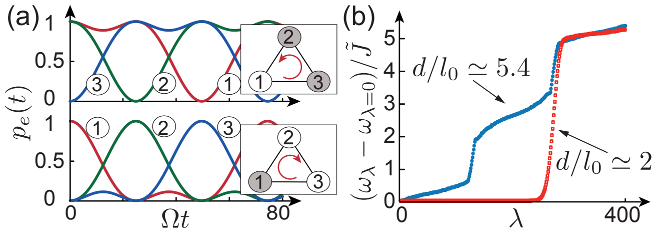


FIG. 4. (a) Evolution of the excited state populations $p_e^n(t)$ of $N = 3$ emitters arranged in a triangle of length $d/l_0 = 4$. For this plot $\ell = 0$, and $\alpha = 1/(16\sqrt{3}) \approx 0.036$, such that the enclosed effective flux is $\theta_\triangle \simeq \pi/2$ and the dipole-dipole interactions become fully chiral (see [34] for details). In the upper panel the initial state contains two excitations in emitter 1 and 2. In the lower panel the initial state contains just one excitation in emitter 1. (b) Single-excitation spectrum of $H_{\rm eff}$ for a square lattice of $20 \times 20$ emitters and normalized to the nearest-neighbor coupling strength $\tilde{J} = |\tilde{J}_{12}|$. The two spectra are obtained for the spacings $d/l_0 = 2$ ($\alpha_{\rm eff} = 0.32$) and $d/l_0 = 5.39$ ($\alpha_{\rm eff} = 2.32$) and in both cases $\alpha = 0.08$ and $\ell = 0$ has been assumed.

arise very naturally from the coupling of emitters to a magnetic photonic reservoir.

We emphasize that the strong coupling of superconducting qubits to arrays of microwave resonators in the regime $g \gg \gamma_e, \gamma_p$ [9, 20, 48] as well as the implementation of synthetic fields in small [29] and large two-dimensional [12] photonic lattices have already been demonstrated. A combination of these techniques is sufficient to probe all the characteristic properties of LPPs with state-of-the-art parameters [34]. With further developments, similar experiments should also become possible with atoms or solid-state emitters coupled to topological lattices in the optical regime [23, 30, 49, 50].

*Conclusions.*—In summary, we have shown how the presence of synthetic magnetic fields changes the physics of light-matter interactions in the bulk of 2D photonic lattices. For moderate magnetic fields this physics can be very accurately described in terms of LPPs, which share the nonlinearity of the matter component and the chiral properties of Landau photons. In the many emitter case, our platform naturally allows the quantum simulation of various interaction-dominated topological systems, which do not appear in electronic systems with only nearest-neighbor interactions.

## ACKNOWLEDGMENTS

We thank Giuseppe Calajo and Francesco Ciccarello for stimulating discussions. This work was supported by the Austrian Academy of Sciences (ÖAW) through a DOC Fellowship (D.D.) and by the Austrian Science Fund (FWF) through the DK CoQuS (Grant No. W 1210) and Grant No. P31701 (ULMAC). We acknowledge financial support from the European Union FET-Open grant "MIR-BOSE" (n.737017), from the H2020-FETFLAG-2018-2020 project "PhoQuS" (n.820392), from the Provincia Autonoma di Trento, from the Q@TN initiative, from Google via the quantum NISQ award, and from AFOSR MURI FA9550-19-1-0399 and ARO MURI W911NF-15-1-0397.

[1] K. von Klitzing, T. Chakraborty, P. Kim, V. Madhavan, X. Dai, J. McIver, Y. Tokura, L. Savary, D. Smirnova, A. M. Rey, C. Felser, J. Gooth, and X. Qi, 40 years of the quantum Hall effect, Nat. Rev. Phys. **2**, 397, (2020).
[2] R. Feynman, *The Feynman Lectures on Physics Vol. III Ch. 21: The Schrödinger Equation in a Classical Context: A Seminar on Superconductivity, Section 21-7: Flux quantization*, www.feynmanlectures.caltech.edu, (2020).
[3] N. Goldman, J. C. Budich, and P. Zoller, Topological quantum matter with ultracold gases in optical lattices, Nat. Phys. **12**, 639 (2016).
[4] N. R. Cooper, J. Dalibard, and I. B. Spielman, Topological bands for ultracold atoms, Rev. Mod. Phys. **91**, 015005 (2019).
[5] T. Ozawa, H. M. Price, A. Amo, N. Goldman, M. Hafezi, L. Lu, M. C. Rechtsman, D. Schuster, J. Simon, O. Zilberberg, and I. Carusotto, Topological photonics, Rev. Mod. Phys. **91**, 015006 (2019).
[6] I. Carusotto, A. A. Houck, A. J. Kollar, P. Roushan, D. I. Schuster, and J. Simon, Photonic materials in circuit quantum electrodynamics, Nat. Phys. **16**, 268 (2020).
[7] V. Peano, C. Brendel, M. Schmidt, and F. Marquardt, Topological Phases of Sound and Light, Phys. Rev. X **5**, 031011 (2015).
[8] S. Barik, A. Karasahin, C. Flower, T. Cai, H. Miyake, W. DeGottardi, M. Hafezi, and E. Waks, A topological quantum optics interface, Science **359**, 6376 (2018).
[9] E. Kim, X. Zhang, V. S. Ferreira, J. Banker, J. K. Iverson, A. Sipahigil, M. Bello, A. Gonzalez-Tudela, M. Mirhosseini, and O. Painter, Quantum electrodynamics in a topological waveguide, arXiv:2005.03802
[10] J. Ningyuan, C. Owens, A. Sommer, D. Schuster, and J. Simon, Time- and Site-Resolved Dynamics in a Topological Circuit, Phys. Rev. X **5**, 021031 (2015).
[11] B. M. Anderson, R. Ma, C. Owens, D. I. Schuster, and J. Simon, Engineering Topological Many-Body Materials in Microwave Cavity Arrays, Phys. Rev. X **6**, 041043, (2016).
[12] C. Owens, A. LaChapelle, B. Saxberg, B. M. Anderson, R. Ma, J. Simon, and D. I. Schuster, Quarter-flux Hofstadter lattice in a qubit-compatible microwave cavity array, Phys. Rev. A **97**, 013818, (2018).
[13] M. Bello, G. Platero, J. I. Cirac, and A. Gonzalez-Tudela, Unconventional quantum optics in topological waveguide QED, Science Adv. **5**, eaaw0297 (2019).
[14] I. García-Elcano, A. González-Tudela, and J. Bravo-Abad, Quantum electrodynamics near photonic Weyl points, Phys. Rev. Lett. **125**, 163602 (2020).

[15] S. Longhi, Quantum decay in a topological continuum, Phys. Rev. A **100**, 022123 (2019).

[16] G. L. Giorgi, S. Lorenzo, and S. Longhi, Topological Protection and Control of Quantum Markovianity, Photonics **7**, 18 (2020).

[17] M. Lemonde, V. Peano, P. Rabl, and D. G. Angelakis, Quantum state transfer via acoustic edge states in a 2D optomechanical array, New J. Phys. **21**, 113030 (2019).

[18] L. Leonforte, A. Carollo, and F. Ciccarello, Vacancy-like dressed states in topological waveguide QED, arXiv:2007.02949 (2020).

[19] N.Y. Yao, C. R. Laumann, A.V. Gorshkov, H. Weimer, L. Jiang, J. I. Cirac, P. Zoller, and M.D. Lukin, Topologically protected quantum state transfer in a chiral spin liquid, Nat. Commun. **4**, 1585 (2013).

[20] I. S. Besedin, M. A. Gorlach, N. N. Abramov, I. Tsitsilin, I. N. Moskalenko, A. A. Dobronosova, D. O. Moskalev, A. R. Matanin, N. S. Smirnov, I. A. Rodionov, A. N. Poddubny, and A. V. Ustinov, Topological photon pairs in a superconducting quantum metamaterial, arXiv:2006.12794 (2020).

[21] A. V. Poshakinskiy, J. Zhong, Y. Ke, N. A. Olekhno, C. Lee, Y. S. Kivshar, and A. N. Poddubny, Quantum Hall phase emerging in an array of atoms interacting with photons, arXiv:2003.08257 (2020).

[22] X. Wang, T. Liu, A. Frisk Kockum, H.-R. Li, and F. Nori, Tunable Chiral Bound States with Giant Atoms, arXiv:2008.13560 (2020).

[23] S. Mittal, J. Fan, S. Faez, A. Migdall, J. M. Taylor, and M. Hafezi, Topologically Robust Transport of Photons in a Synthetic Gauge Field, Phys. Rev. Lett. **113**, 087403 (2014).

[24] P. Lodahl, S. Mahmoodian, S. Stobbe, A. Rauschenbeutel, P. Schneeweiss, J. Volz, H. Pichler, and P. Zoller, Chiral quantum optics, Nature **541**, (2017).

[25] L. Page, Deflection of Electrons by a Magnetic Field on the Wave Mechanics, Phys. Rev. **36**, 444 (1930).

[26] S. M. Girvin, The Quantum Hall Effect: Novel Excitations and Broken Symmetries, arXiv:cond-mat/9907002

[27] See Ref. [18] for a related type of circulating bound state in the Haldane mode.

[28] K. Fang, Z. Yu, and S. Fan, Realizing effective magnetic field for photons by controlling the phase of dynamic modulation, Nat. Photon. **6**, 782 (2012).

[29] P. Roushan, C. Neill, A. Megrant, Y. Chen, R. Babbush, R. Barends, B. Campbell, Z. Chen, B. Chiaro, A. Dunsworth, A. Fowler, E. Jeffrey, J. Kelly, E. Lucero, J. Mutus, P. J. J. O'Malley, M. Neeley, C. Quintana, D. Sank, A. Vainsencher, J. Wenner, T. White, E. Kapit, H. Neven, and J. Martinis, Chiral ground-state currents of interacting photons in a synthetic magnetic field, Nat. Phys. **13**, 146 (2017).

[30] M. Hafezi, S. Mittal, J. Fan, A. Migdall, and J. M. Taylor, Imaging topological edge states in silicon photonics, Nat. Photon. **7**, 1001 (2013).

[31] H. Ren, T. Shah, H. Pfeifer, C. Brendel, V. Peano, F. Marquardt, and O. Painter, Topological phonon transport in an optomechanical system, arXiv:2009.06174 (2020).

[32] J. Koch, A. A. Houck, K. Le Hur, and S. Girvin, Time-reversal-symmetry breaking in circuit-QED-based photon lattices. Phys. Rev. A **82**, 043811 (2010).

[33] D. R. Hofstadter, Energy levels and wave functions of Bloch electrons in rational and irrational magnetic fields, Phys. Rev. B **14**, 2239 (1976).

[34] See the Supplementary Material, which additionally includes Refs. [35–43], for a more detailed derivation of all the analytic results.

[35] F. Harper, S. H. Simon, and R. Roy, Perturbative approach to flat Chern bands in the Hofstadter model, Phys. Rev. B **90**, 075104 (2014).

[36] T. Ueta, Lattice Green function in uniform magnetic fields, J. Phys. A **30**, 15 (1997).

[37] K. E. Cahill and R. J. Glauber, Ordered Expansions in Boson Amplitude Operators, Phys. Rev. **177**, 1857 (1969).

[38] T. Ueta, Green's Function of a Charged Particle in Magnetic Fields, J. Phys. Soc. Jap. **61**, 4314 (1992).

[39] R. Alicki, J. R. Klauder, and J. Lewandowski, Landau-level ground-state degeneracy and its relevance for a general quantization procedure, Phys. Rev. A **48**, 2538 (1993).

[40] F. F. Assaad and S. Biskamp, Fractional quantum Hall effect on a lattice, Phys. Rev. B **51**, 1605 (1995).

[41] A. Gonzalez-Tudela and J. I. Cirac, Markovian and non-Markovian dynamics of quantum emitters coupled to two-dimensional structured reservoirs, Phys. Rev. A **96**, 043811 (2017).

[42] M. Mirhosseini, E. Kim, V. S. Ferreira, M. Kalaee, A. Sipahigil, A. J. Keller, and O. Painter, Superconducting metamaterials for waveguide quantum electrodynamics, Nat. Com. **9**, 3706 (2018).

[43] R. Ma, B. Saxberg, C. Owens, N. Leung, Y. Lu, J. Simon, and D. I. Schuster, A dissipatively stabilized Mott insulator of photons, Nature **566**, 51 (2019).

[44] G. Calajo, F. Ciccarello, D. Chang, and P. Rabl, Atom-field dressed states in slow-light waveguide QED Phys. Rev. A **93**, 033833 (2016).

[45] B. I. Halperin, Quantized Hall conductance, current-carrying edge states, and the existence of extended states in a two-dimensional disordered potential, Phys. Rev. B **25**, 2185 (1982).

[46] M. Tavis, and F. W. Cummings, Exact Solution for an N-Molecule Radiation-Field Hamiltonian, Phys. Rev. **170**, 379 (1968).

[47] E. Kapit and E. Mueller, Exact Parent Hamiltonian for the Quantum Hall States in a Lattice, Phys. Rev. Lett. **105**, 215303 (2010).

[48] Y. Liu and A. A. Houck, Quantum electrodynamics near a photonic bandgap, Nat. Phys. **13**, 48 (2016).

[49] S. Mittal, E. A. Goldschmidt, and M. Hafezi, A topological source of quantum light, Nature **561**, 502 (2018).

[50] S. Barik, A. Karasahin, S. Mittal, E. Waks, and M. Hafezi, Chiral quantum optics using a topological resonator, Phys. Rev. B **101**, 205303 (2020).